Available online at www.sciencedirect.com

ScienceDirect

Microelectronic Engineering 85 (2008) 768–773

MICROELECTRONIC ENGINEERING

www.elsevier.com/locate/mee

E-beam lithography of catalyst patterns for carbon nanotube growth on insulating substrates

M. Häffner [a,*], A. Haug [b], R.T. Weitz [c], M. Fleischer [a], M. Burghard [c], H. Peisert [b], T. Chassé [b], D.P. Kern [a]

[a] *Institute of Applied Physics, University of Tübingen, Germany*
[b] *Institute of Physical and Theoretical Chemistry, University of Tübingen, Germany*
[c] *Max-Planck-Institute for Solid State Research, Stuttgart, Germany*

Received 5 October 2007; received in revised form 14 January 2008; accepted 15 January 2008
Available online 26 January 2008

Abstract

We present a process for fabricating small catalyst particles for carbon nanotube growth on insulating substrates. For this purpose we define hydrogen silsesquioxane (HSQ) resist structures on top of conducting and grounded metallic catalyst layers and a sacrificial chromium layer, using e-beam lithography.

The developed resist structures act as an etch mask in the subsequent ion milling step, by which the surrounding metal layers are removed. Having wet etched the Cr mask and HSQ resist, metal structures remain which serve as catalyst in a chemical vapour deposition (CVD) process resulting in single wall carbon nanotubes with a diameter range of 0.8–2.0 nm on insulating substrates.

Keywords: Carbon nanotube; CNT; Catalyst; HSQ; Ion milling; CVD; Electron beam; Insulating

1. Introduction

Optical absorption spectroscopy is an important method for characterizing electronic properties of carbon nanotubes, complementing Raman measurements and transmission electron microscopy [1]. Here substrates which are transmitting in the range of ultraviolet (UV) and visible light (VIS) like quartz glass have to be used. Furthermore, opto-electronic applications of carbon nanotube devices require a flexible choice of substrates [2,3]. However, quartz glass is not conductive and thus cannot be used for the fabrication of catalyst patterns in standard e-beam lift-off processes without the addition of a conductive layer [4] on top of the resist. Other methods of e-beam lithography on insulating substrates are limited by the critical energy of the electron beam [5], the resolution of the resist [6] or the remaining conductive layer after lift-off [7,8]. Thus up to the present only large catalyst areas with dimensions of several tens of microns have been patterned on insulating substrates [2,9]. However, controlling the size of the catalyst down to the nanometer scale is a key issue for selective carbon nanotube growth, which we address in this work.

We present a modified e-beam lithography process [9] in which high resolution patterns are defined in hydrogen silsesquioxane (HSQ) and etched into an underlying catalyst layer. This process has the advantage that the conducting continuous metal stack enables the fabrication of nanoscale catalyst particles on insulating substrates.

2. Fabrication

In our process we extend the fabrication method presented in [10] to the fabrication of catalyst patterns for carbon nanotube growth. The fabrication process is described

---

[*] Corresponding author.
E-mail address: michael.haeffner@web.de (M. Häffner).

0167-9317/$ - see front matter © 2008 Elsevier B.V. All rights reserved.
doi:10.1016/j.mee.2008.01.046

in Fig. 1. As a catalyst 10.0 nm Al, 1.0 nm Fe, and 0.2 nm Mo [11] are vacuum deposited on the substrate. On the top of the catalyst layers a 7.0 nm sacrificial layer of Cr is evaporated. Afterwards, an additional layer consisting of hydrogen silsesquioxane (HSQ) – a negative tone e-beam resist (Fig. 1a) – is added via spin coating.

By exposing the resist via electron beam (Fig. 1b), using the underlying metal as a grounded conducting layer and developing the resist in tetramethyl ammonium hydroxide (TMAH) (Fig. 1c) for 60 s, structures with dimensions of few tens of nanometers as well as larger patterns, e.g. for optical spectroscopy, can be fabricated. In contrast to the procedures presented earlier [12,13], the resist is developed without using elevated development temperatures since we do not want to inadvertently etch the catalyst layers. After development, the samples are dried supercritically in order to prevent pattern collapse due to the capillary forces. The developed HSQ is used as an etch mask for the subsequent ion milling step, by which the surrounding metal layers are removed (Fig. 1d). Due to the dependence of the milling rate on the angle of incidence of the ions and to erosion at the edges of the HSQ etch mask, the etching profile has a finite side-wall angle. Thus by using e.g. dots as an etch mask, the resulting catalyst structure is a truncated cone for larger diameter dots or a cone for small dots. Finally, the HSQ is lifted off by wet etching the chromium layer (Fig. 1e). Carbon nanotubes can be grown by CVD on the patterned catalyst (Fig. 1f).

3. Ion milling and chromium wet etching

The catalyst layer, consisting of 10.0 nm Al, 1.0 nm Fe and 0.2 nm Mo, and the 7.0 nm sacrificial Cr layer are etched by Ar ion milling using exposed and developed

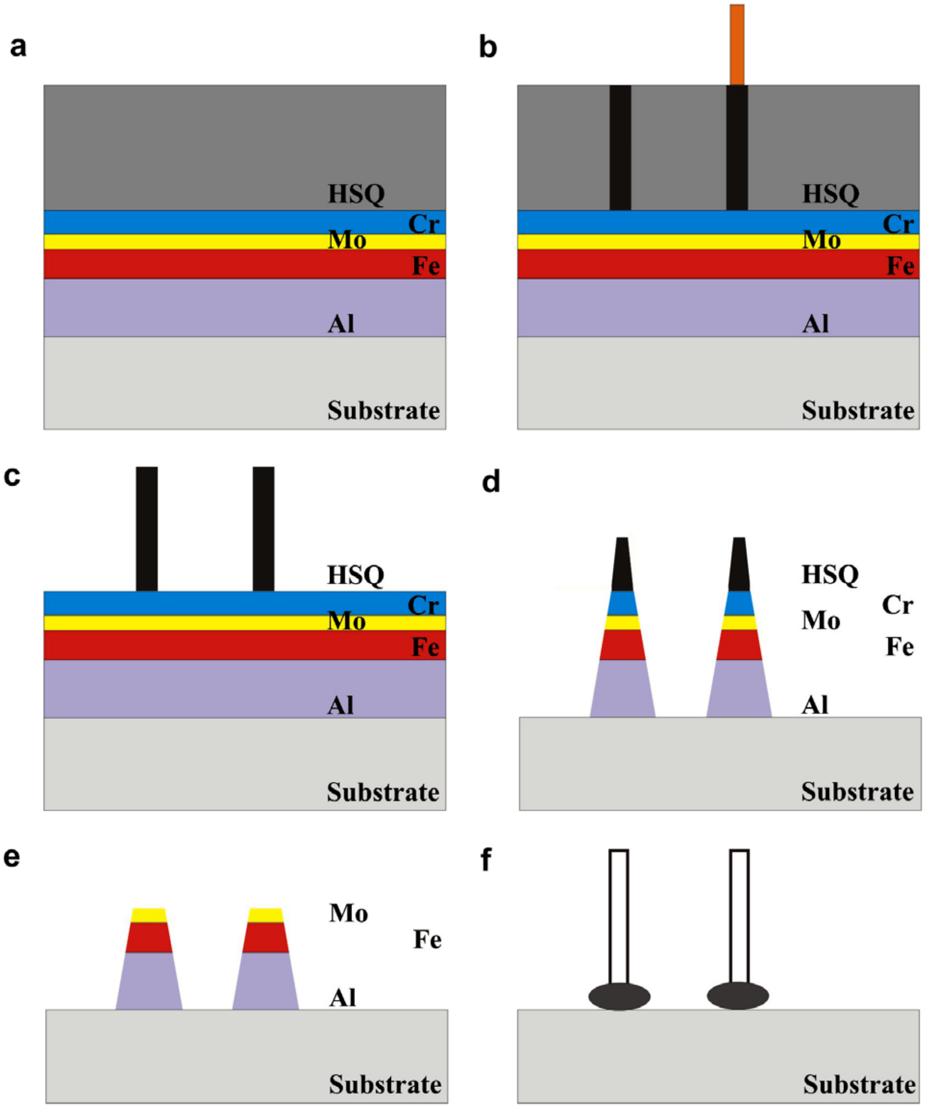

Fig. 1. Fabrication process of the catalyst particles. (a) Catalyst stack and e-beam resist (HSQ) on top of an insulating substrate. (b) Exposure of the resist. Charging is prevented by grounding the underlying metal layers. (c) Development of the resist in TMAH. (d) Ion milling. (e) Cr wet etching. (f) CVD carbon nanotube growth.

Table 1
Melting points, atomic densities, and etch rates of the materials that are being etched

	Melting point (K)	Atomic density of the target material (10^{22} atoms/cm^3)	Etch rate (nm/min [bulk])
HSQ	1200	1.6	14
Mo	2896	6.4	4
Cr	2130	8.3	4
Fe	1808	8.5	5
Al	933	6.0	8

All etch rates are measured from samples etched at 700 V, using 0.7 mA/cm^2 Ar ions

HSQ resist as an etch mask. According to [14] the etching, which is a sputtering process, results from the transfer of momentum from the incident ions to the target atoms. The etch rate $V(\Theta)$, measured in nm/min can be derived from the sputtering yield $S(\Theta)$:

$$V(\Theta) = 9.6 \times 10^{24} \times \frac{J}{\mathrm{mA/cm^2}} \frac{S(\Theta)}{n} \cos\Theta \left[\frac{\mathrm{nm}}{\mathrm{min}}\right] \quad (1)$$

where n is the atomic density of the target material in atoms/cm^3, J is the current density in mA/cm^2 and the $\cos\Theta$ term accounts for the reduced current density at angles to the normal. The sputtering yield S bears a relation

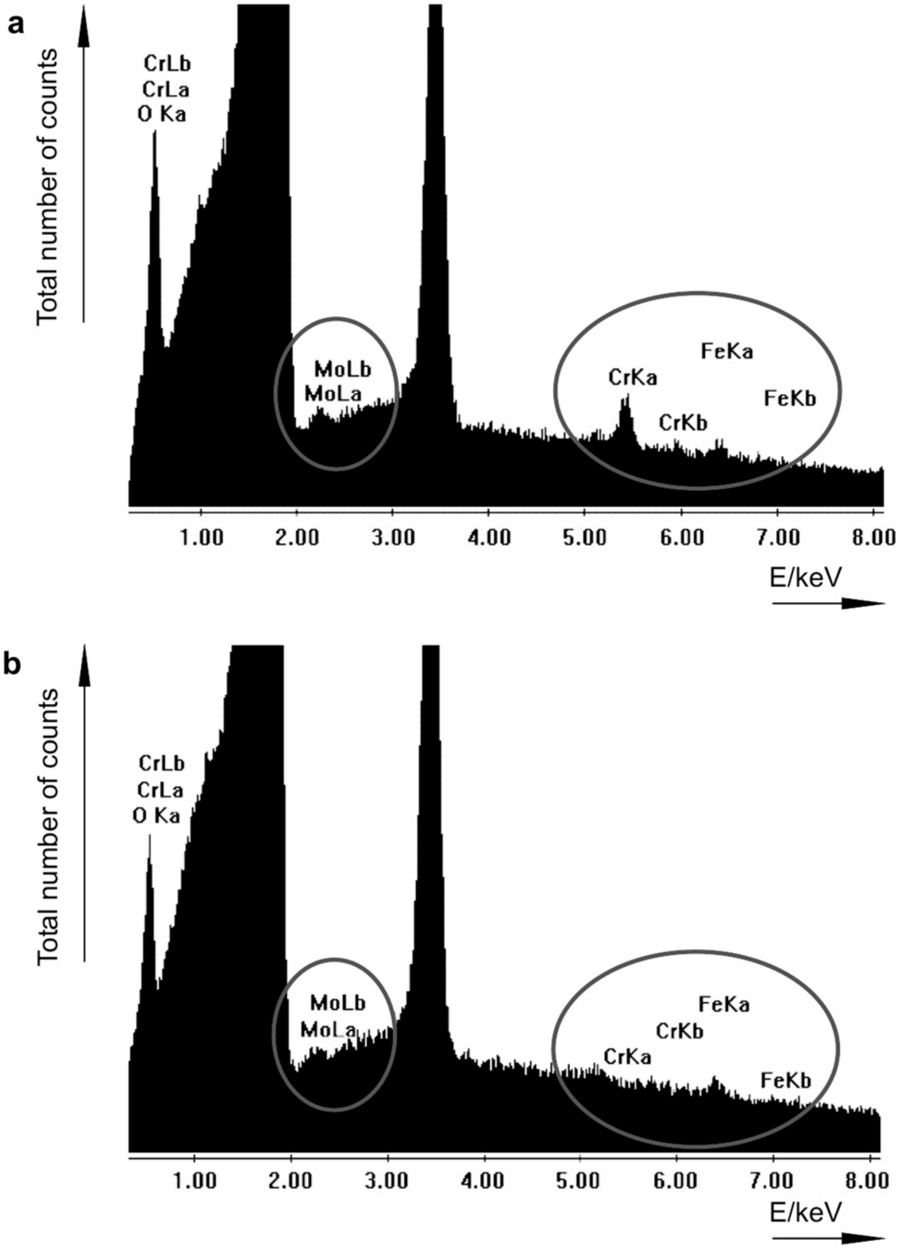

Fig. 2. EDX spectra that are used to control the etching processes by repeatedly checking the presence of the materials at the exposed positions. (a) Presence of Cr after ion milling shows the integrity of the underlying catalyst stack. (b) After Cr wet etching Cr is removed but Fe and Mo are still present, indicating the end of the wet etching process.

to the binding energy of the sample atoms [15], which in turn is related to the melting point of the material being etched and increases with increasing energy. For angles below 30–40° $S(\theta) \sim 1/\cos(\theta)$. We etch at an angle of 0°, using 0.7 mA/cm^2 Ar ions at 700 V. In order to prevent charging, we neutralize the ions before hitting the sample. Table 1 shows the melting point, the atomic density, and the experimentally determined etch rates of the materials used. The tendency of increasing etch rates with both decreasing melting point and decreasing atomic density can be clearly seen. Thus the knowledge of the key parameters melting point and atomic density of a material allows to estimate the etch rate of this material by comparing these parameters to materials with an already determined etch rate. Using these trends, the corresponding etch mask thickness can be designed. Overetching during ion milling and chromium wet etching is an important process parameter and can be controlled by repeatedly checking the remaining elements in an energy dispersive X-ray (EDX) spectrum. Fig. 2 shows two EDX spectra before (a) and after (b) chromium wet etching. Especially by watching the chromium peak, overetching can be controlled. However, in our case the HSQ etch mask is made very thick. It takes about 4 min to etch the metal stack, whereas the 140 nm thick HSQ resist could last for 10 min and the etch rate standard deviation of our ion milling process is only approximately 10%. Hence overetching of more than a factor of two in order to etch the surrounding catalyst stack with certainty is uncritical. Whether chromium wet etching is critical depends on the underlying catalyst layer. In our case it is possible to apply the chromium wet etch two times longer than it would be necessary for the 7 nm chromium layer without evidently etching the underlying catalyst stack. Thus, repeatedly checking remaining elements in an EDX spectrum is very helpful during process development, but can be avoided, once all etch rates are determined and corresponding layer thicknesses are designed.

4. Results and discussion

Fig. 3 shows the fabricated catalyst patterns after each of the aforementioned process steps, using an insulating layer of 190 nm SiO_2 on Si as a substrate. Exposed and developed HSQ pillars on the metal stack can be seen in Fig. 3a. The HSQ pillars have a diameter range of 30–500 nm. After ion milling (Fig. 3b) the HSQ pillars are reduced in size, and the thin surrounding metal layers are removed. Having wet etched the Cr mask and HSQ resist (Fig. 3c), circular Al–Fe–Mo dots remain which serve as catalyst in the subsequent CVD process, yielding long single carbon nanotubes originating from individual dots (Fig. 3d). In our case CVD growth is performed at 900 °C using ethanol as the carbon source and resulting in a low density of single wall carbon nanotubes for nanotube transistor fabrication.

It has thus been demonstrated by the example of an SiO_2 substrate, that small catalyst particles for carbon nanotube

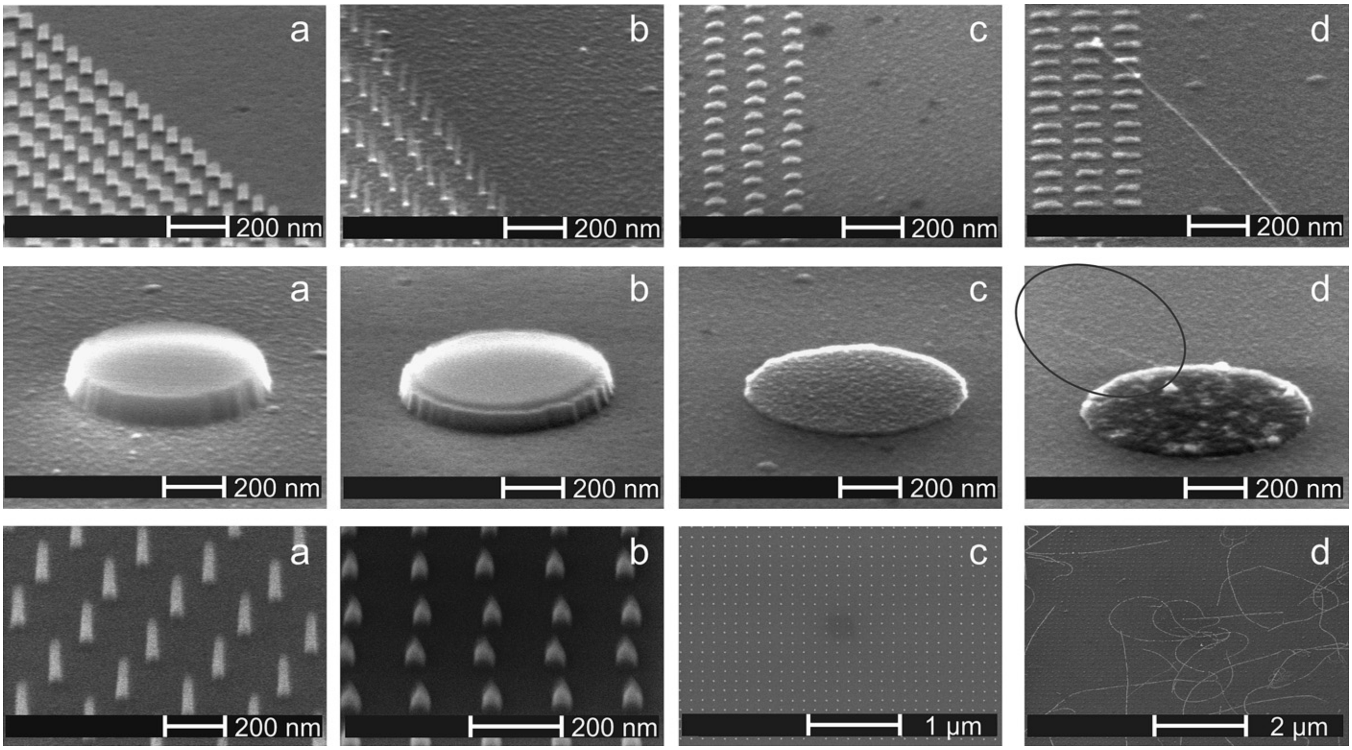

Fig. 3. Illustration of the fabrication process after (a) exposure and development, (b) ion milling, (c) chromium wet etching, and (d) CVD nanotube growth.

growth can be defined on insulating substrates using e-beam lithography.

Using the same process on a transparent, insulating quartz glass substrate, Raman spectra of carbon nanotubes (Fig. 4), grown from unpatterned catalyst (A) and patterned catalyst (B), demonstrate by the presence of radial breathing modes that in either case single wall carbon nanotubes (SWNTs) can be grown. The experiments were performed with a Nd:YAG laser line at 532.14 nm (2.33 eV) in the backscattering geometry. Here the unpatterned catalyst consists of the Al–Fe–Mo metal stack with aforementioned thicknesses evaporated on a quartz glass substrate. The radial breathing mode (RBM, left spectrum, 100–250 cm^{-1}) is the fingerprint region of the SWNTs. For

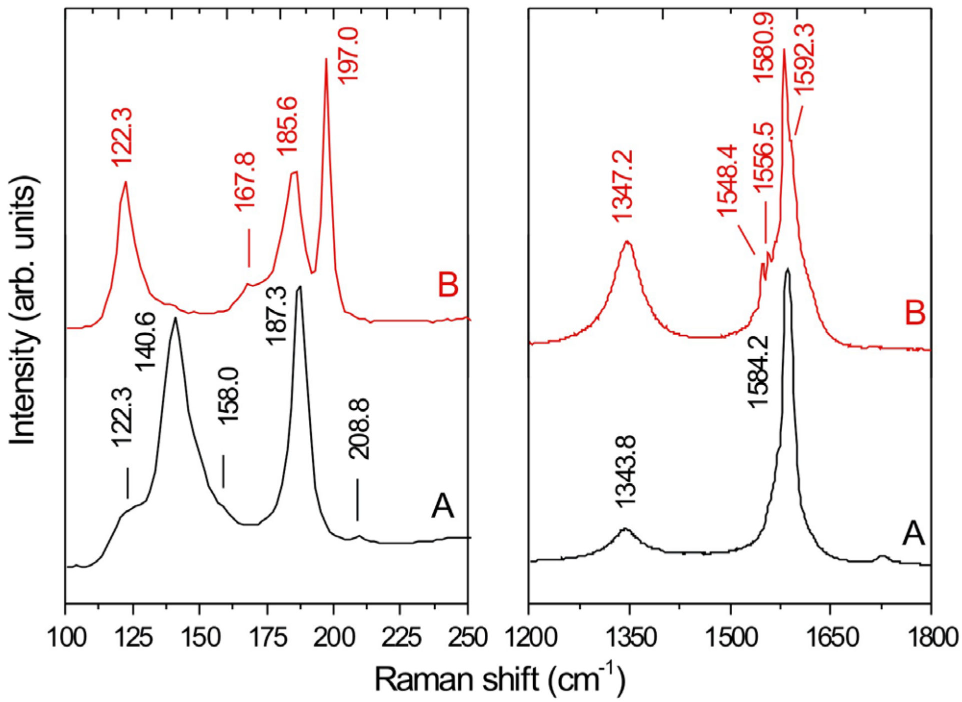

Fig. 4. Raman spectra of carbon nanotubes grown from unpatterned (A) and patterned (B) catalyst.

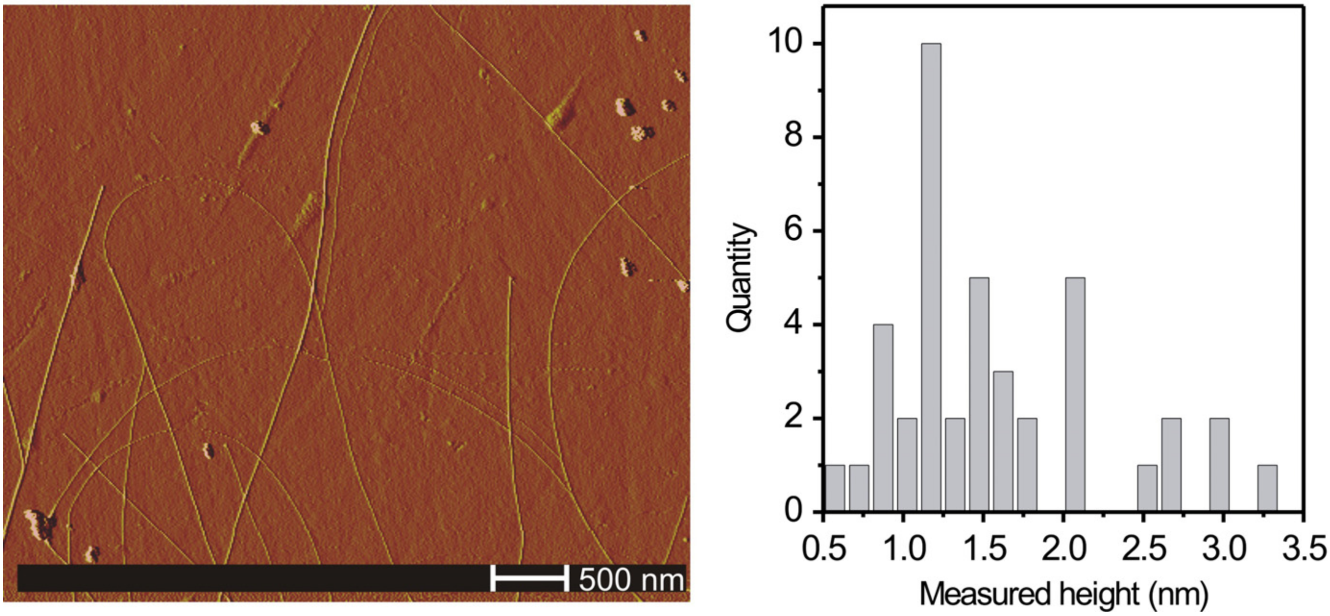

Fig. 5. Tapping mode atomic force microscopy (AFM) amplitude image, demonstrating the growth of carbon nanotubes on a quartz glass substrate (left). Apparent heights of 40 carbon nanotubes (right). It is interesting to note that 25% of all the carbon nanotubes found have an apparent height of 1.2 ± 0.1 nm. The values measured by AFM are in good agreement with the diameter range determined by the Raman measurements.

our samples, the bands can be assigned to a diameter range of 0.8–2.0 nm, since the frequency is related to the diameter d of the nanotube, i.e. each peak in the left spectrum (100–250 cm^{-1}) corresponds to a certain single wall nanotube diameter according to $\omega_{\mathrm{RBM}} = A/d + B$ with $A = 204\ \mathrm{cm}^{-1}$ and $B = 27\ \mathrm{cm}^{-1}$ [16]. Since different samples show varying nanotube diameters, the Raman spectrum in the fingerprint region (left spectrum) shows different RBM-peaks for sample A (unpatterned catalyst) and B (patterned catalyst). Another important region in the Raman spectrum of SWNTs is the region from 1200 to 1800 cm^{-1}, which shows lines that are related to ordered (D line, 1343.8 cm^{-1} (A) and 1347.2 cm^{-1} (B)) and disordered (G line, 1584.2 cm^{-1} (A) and 1580 cm^{-1} (B)) graphite vibration modes [17,18]. The ratio of these bands describes the status of the chemical conversion of educts to the expected product and hence the quality of the CVD-grown CNTs. As further proof, the atomic force microscope (AFM) image in Fig. 5 (left) shows the corresponding carbon nanotubes on the quartz glass substrate. The apparent heights of 40 nanotubes (right) are in good agreement with the diameter range as determined by the Raman measurements.

5. Conclusions

In conclusion, a fabrication process for structuring catalyst particles with dimensions of several tens of nanometers for carbon nanotube growth on insulating substrates has been developed, using e-beam lithography. Using the catalyst metal stack and a sacrificial chromium layer as a conducting layer thereby avoids charging of the substrate. The application of HSQ as a negative tone e-beam resist allows the fabrication of high resolution nanopatterns that are transferred into the underlying catalyst stack using ion milling. Raman spectra and AFM images demonstrate, that single wall carbon nanotubes with a diameter range of 0.8–2.0 nm can be grown on patterned quartz substrates.

The advantage of this e-beam fabrication process is the ability to structure HSQ resist which yields high resolution patterns on an insulating substrate, and the ability to subtractively craft the catalyst particles from a continuous film, which enables high control over the achieved structures by repeatedly controlling the progress of ion milling.

Acknowledgements

Financial support from the Landesstiftung Baden Württemberg within the “Kompetenznetz funktionelle Nanostrukturen” and from the Ministerium für Wissenschaft, Forschung und Kunst Baden-Württemberg, AZ 24-7535.23-21.18, is gratefully acknowledged.

References

[1] H. Kataura, Y. Kumazawa, Y. Maniwa, I. Umezu, S. Suzuki, Y. Ohtsuka, Y. Achiba, Synth. Met. 103 (1999) 2555.
[2] H. Murakami, M. Hirakawa, C. Tanaka, H. Yamakawa, Appl. Phys. Lett. 76 (2000) 1776.
[3] Z.F. Ren, Z.P. Huang, J.W. Xu, J.H. Wang, P. Bush, M.P. Siegal, P.N. Provencio, Science 282 (1998) 1105.
[4] G. Piaszenski, U. Barth, A. Rudzinski, A. Rampe, A. Fuchs, M. Bender, U. Plachetka, Microelectron. Eng. 84 (2007) 945.
[5] J. Joo, B.Y. Chow, J.M. Jacobson, Nano Lett. 6 (2006) 2021.
[6] M.A.Z. Hupcey, C.K. Ober, J. Vac. Sci. Technol. B 16 (1998) 3701.
[7] G. Dolling, C. Enkrich, M. Wegener, J. Zhou, C. M. Soukoulis, S. Linden, arxiv:/arXiv:physics/0507045v1 (2005).
[8] X. Xia, H. Yang, Z. Wang, Y. Li, Z. Cui, Y. Chen, C. Gu, Microelectron. Eng. 84 (2007) 1144.
[9] E.J. Bae, Y.-S. Min, U. Kim, W. Park, Nanotechnology 18 (2007) 15601.
[10] F. Stade, A. Heeren, M. Fleischer, D.P. Kern, Microelectron. Eng. 84 (2007) 1589.
[11] L. Delzeit, B. Chen, A. Cassell, R. Stevens, C. Nguyen, M. Meyyappan, Chem. Phys. Lett. 348 (2001) 368.
[12] M. Häffner, A. Heeren, M. Fleischer, D.P. Kern, G. Schmidt, L.W. Molenkamp, Microelectron. Eng. 84 (2007) 937.
[13] M. Häffner, A. Haug, A. Heeren, M. Fleischer, H. Peisert, T. Chassé, D.P. Kern, J. Vac. Sci. Technol. B 25 (2007) 2045.
[14] S. Somekh, J. Vac. Sci. Technol. 13 (1976) 1003.
[15] E.G. Spencer, P.H. Schmidt, J. Vac. Sci. Technol. 8 (1971) 52.
[16] J.C. Meyer, M. Paillet, T. Michel, A. Moreac, A. Neumann, G.S. Duesberg, S. Roth, J.-L. Sauvajol, Phys. Rev. Lett. 95 (2005) 217401.
[17] A.M. Rao, E. Richter, S. Bandow, B. Chase, P.C. Eklund, K.A. Williams, S. Fang, K.R. Subbaswamy, M. Menon, A. Thess, R.E. Smalley, G. Dresselhaus, M.S. Dresselhaus, Science 275 (1997) 187.
[18] H. Kuzmany, W. Plank, M. Hulman, Ch. Kramberger, A. Grüneis, Th. Pichler, H. Peterlik, H. Kataura, Y. Achiba, Eur. Phys. J. B 22 (2001) 307.